JCTC Journal of Chemical Theory and Computation

Article

pubs.acs.org/JCTC

Why Do TD-DFT Excitation Energies of BODIPY/Aza-BODIPY Families Largely Deviate from Experiment? Answers from Electron Correlated and Multireference Methods

Mohammad R. Momeni and Alex Brown*

Department of Chemistry, University of Alberta, Edmonton, Alberta T6G 2G2, Canada

Supporting Information

ABSTRACT: The vertical excitation energies of 17 boron−dipyrromethene (BODIPY) core structures with a variety of substituents and ring sizes are benchmarked using time-dependent density functional theory (TD-DFT) with nine different functionals combined with the cc-pVTZ basis set. When compared to experimental measurements, all functionals provide mean absolute errors (mean AEs) greater than 0.3 eV, larger than the 0.1−0.3 eV differences typically expected from TD-DFT. Due to the high linear correlation of TD-DFT results with experiment, most functionals can be used to predict excitation energies if corrected empirically. Using the CAM-B3LYP functional, 0−0 transition energies are determined, and while the absolute difference is improved (mean AE = 0.478 eV compared to 0.579 eV), the correlation diminishes substantially (R^2 = 0.961 to 0.862). Two very recently introduced charge transfer (CT) indices, q^{CT} and d^{CT}, and electron density difference (EDD) plots demonstrate that CT does not play a significant role for most of the BODIPYs examined and, thus, cannot be the source of error in TD-DFT. To assess TD-DFT methods, vertical excitation energies are determined utilizing TD-HF, configuration interaction CIS and CIS(D), equation of motion EOM-CCSD, SAC-CI, and Laplace-transform based local coupled-cluster singles and approximate doubles LCC2* methods. Moreover, multireference CASSCF and CASPT2 vertical excitation energies were also obtained for all species (except CASPT2 was not feasible for the four largest systems). The SAC-CI/cc-pVDZ, LCC2*/cc-pVDZ, and CASPT2/cc-pVDZ approaches are shown to have the smallest mean AEs of 0.154, 0.109, and 0.100 eV, respectively; the utility of the LCC2* approach is demonstrated for eight extended BODIPYs and aza-BODIPYs. We found that the problems with TD-DFT arise from difficulties in dealing with the differential electron correlation (as assessed by comparing CCS, CC2, LR-CCSD, CCSDR(T), and CCSDR(3) vertical excitation energies for five compounds) and from contributions of multireference character and double excitations (from analysis of the CASSCF wave functions).

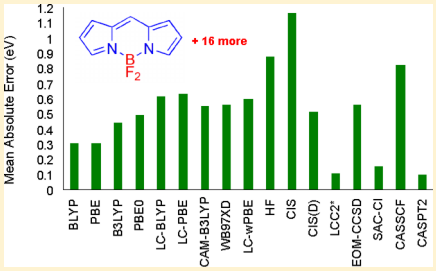

1. INTRODUCTION

Boron−dipyrromethenes (known as BODIPYs), where boron difluoride is attached to conjugated dipyrromethene, are a very important class of organic fluorophores; see Figure 1 for examples of the BODIPY structures. Despite their small sizes and relatively simple structures, they exhibit excellent photophysical properties such as high extinction coefficients and quantum yields.[1,2] Moreover, their photophysical properties, e.g., absorption and emission wavelengths, can be tuned via carefully chosen chemical modification. Due to their excellent properties, BODIPYs find use in a wide range of applications such as photodynamic therapy,[3,4] electrochemistry and electrogenerated chemiluminescence,[5] laser dyes,[6,7] labeling and fluorescent indicators and probes,[8,9] imaging and sensing[10,11] and singlet oxygen generation.[12] The first report of the synthesis of BODIPYs goes back to 1968 by Treibs and Kreuzer.[13] Interestingly, the X-ray structure of the fully unsubstituted system, i.e., the parent BODIPY compound (**1**), was only revealed 41 years later by two separate groups. Schmitt et al. synthesized compound **1** via the reaction of dipyrromethene with boron trifluoride,[14] while Arroyo et al. reported synthesis of this compound by removing the thiomethyl group from the corresponding substituted BODIPY.[15] Although these fundamental studies were only carried out in the past 5 years, extensive experimental and theoretical efforts[1] have been undertaken since the first reported synthesis. From the extensive work carried out, altering the size and/or number of rings in the core BODIPY system or substituting different functional groups can impart significant changes on the absorption and emission wavelengths as well as their photostabilities.[16−19] Extensive effort has been devoted to the design and synthesis of new BODIPY based systems with near IR absorptions and emissions.[20−22] For example, substituted azadipyrromethenes (aza-BODIPY) based systems, where the C−H group at the meso position in the core structure is replaced with a nitrogen atom, constitute a very important class of the red-shifted BODIPY systems.[23] Ideally, one would then like a reliable computational approach for predicting the effects of chemical modification of BODIPYs.

Time-dependent density functional theory (TD-DFT) is the computational method of choice for studying excited state

Received: August 26, 2014
Published: May 4, 2015

DOI: 10.1021/ct500775r
J. Chem. Theory Comput. 2015, 11, 2619−2632

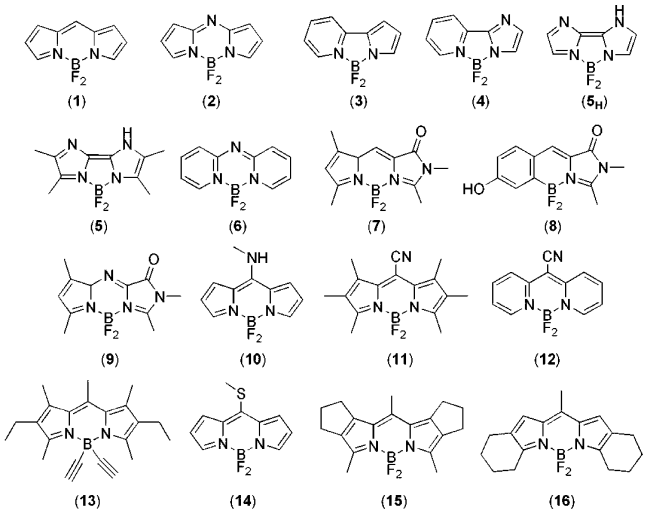

Figure 1. First set of structures considered in this study.

properties in many systems due to its overall accuracy and efficiency; i.e., in most cases, TD-DFT provides adequate accuracy for excitation energies (0.1−0.3 eV difference with experiment) within a reasonable amount of time even for large molecules. However, the TD-DFT approach has some well-known difficulties. For example, TD-DFT results based on standard functionals are often poor when dealing with excitations involving charge transfer (CT) or, more generally, long-range excitations, e.g., in conjugated systems with attached electron donor and acceptor groups. Some of these problems have been mitigated through the introduction of range-separated functionals such as CAM-B3LYP and ωB97X-D. Second, DFT, and, hence, TD-DFT, encounters difficulties when the ground (and/or excited state) has multireference character. Finally, because TD-DFT is a single-electron theory, it cannot handle double excitations in its standard form. Many of the issues with TD-DFT can be attributed to the underlying approximations, i.e., the adiabatic approximation and the requisite use of approximate exchange correlation functionals.[24] Alternatively, highly correlated multireference techniques, such as CASSCF as well as methods built from the CASSCF reference including CASPT2 and multireference CI (MRCI), can be utilized to determine the excited states. These methods work well and are able to account for the difficulties with TD-DFT. However, these multireference techniques are not "black box" as one must choose an adequate active space, and, more importantly for BODIPYs, they are not particularly well-suited for large systems. On the other hand, one can tackle excited states using other ab initio methods such as CIS, CIS(D), EOM-CC, SAC-CI, and CC2. In general, these single-reference techniques are reliable, have reasonable accuracy, and can be applied to (relatively) large molecular systems. In the present work, we will assess the relative merits of both TD-DFT and ab initio approaches for determining the lowest lying excited state energy for BODIPYs.

In the search for the best choice of functional to use within TD-DFT for these systems, there have been several TD-DFT benchmark studies on BODIPYs.[23,25−30] To the best of our knowledge, two very recently published works of Jacquemin et al. are the only cases in the literature that tried to provide accurate theoretical estimates and to address the systematic shift (>0.3 eV) of TD-DFT results compared to experiment for a large subclass of BODIPYs.[31,32] In the first study, they proposed a combination of the Bethe−Salpeter approach with TD-DFT for computing vertical absorption and emission energies of oxygen substituted BODIPYs (NBOs).[31] Using this approach, they succeeded in decreasing the mean absolute errors (mean AEs) from 0.25−0.45 eV in the raw TD-DFT to 0.07−0.18 eV in the combined approach for the studied molecules. In the second study, they suggested the use of the scaled opposite-spin variant CIS(D) (SOS-CIS(D) method) for screening both BODIPYs and aza-BODIPYs;[32,33] for seminal works on the spin-component scaled SCS-CIS(D) and SOS-CIS(D) methods, see refs 34 and 35. More specifically, TD-DFT 0−0 energies were corrected with vertical CIS(D) and SOS-CIS(D) energies in which the mean AE was reduced from ca. 0.4 eV for raw 0−0 energies to ca. 0.2 eV for CIS(D) and ca. 0.1 eV for the SOS-CIS(D) approaches. In another very recent study, Petrushenko and Petrushenko studied the effect of substitution in the meso position using TD-DFT and RI-CC2 methods.[36] Le Guennic and Jacquemin have also recently compared TD-DFT, CC2, CC3, CIS(D), ADC(2), and CASPT2 results for the closely related cyanine chains.[37]

The present work attempts to find the trends and connections between different BODIPY and BODIPY-like systems to illustrate the extent of the TD-DFT discrepancy and to understand its source. With these goals in mind, TD-DFT and ab initio, including CASSCF, computations for molecules within these families are presented and compared and contrasted to each other as well as to published experimental measurements. Through evaluation of CT and multireference indices and comparison of methods systematically including higher levels of electron correlation, along with examination of the CASSCF wave functions, the nature of the difficulties with TD-DFT for BODIPYs will be addressed. To reach this goal, a set of 17 different BODIPY systems is chosen to be investigated where 13 of them have been synthesized and experimentally characterized; see Figure 1. In section 2, a summary of the computational methods utilized is provided. Section 3 presents the computational results including optimized ground and excited state geometries, excitation energies, and CT and multireference indices. In section 3.2, TD-DFT vertical excitation energies for all systems will be compared and contrasted with the experimental results to show the extent of the difference for each of the nine functionals considered. Since all TD-DFT results are systematically shifted from, but highly correlated to, the experimental measurements, linear fit equations are derived using the nine DFT functionals to provide empirical corrections to the theoretical predictions. To assess the error introduced by comparing vertical adiabatic excitation energies to the experimental absorption maxima, the 0−0 transition energies were also determined utilizing the CAM-B3LYP functional. As a further point of comparison, the computed spectra of compounds **1** and **14** using all nine different functionals are compared to the available experimental ones. In section 3.3, the computed CAM-B3LYP CT parameters, q^{CT} (amount of the transferred charge) and d^{CT} (CT distance based on the hole−electron distance), along with the electron density difference (EDD) plots are discussed for all species to determine the role of CT in the systematic differences observed for TD-DFT. Section 3.4 is dedicated to the discussion of vertical excitation energies computed using ab initio TD-HF, CIS, CIS(D), EOM-CCSD, SAC-CI, LCC2*, and multireference CASSCF and CASPT2 methods. For a smaller subset of the test molecules, the effects of increasing correlation are examined by determining the excitation energies

DOI: 10.1021/ct500775r
J. Chem. Theory Comput. 2015, 11, 2619−2632

Table 1. CASSCF/CASPT2(n,m) Vertical Excitation Energies[b] (eV) for Different Active Spaces of Compound 1 Using the cc-pVTZ Basis Set in the Gas Phase[a]

CASSCF	[2,2]	[4,4]	[6,6]	[8,8]	[10,10]	[12,11]
energy	3.743	3.717	3.464	3.623	2.837	2.829
deviation	+1.283	+1.257	+1.004	+1.163	+0.377	+0.369
CASPT2	[2,2]	[4,4]	[6,6]	[8,8]	[10,10]	[12,11]
energy	2.056	2.133	2.364	2.416	2.407	2.450
deviation	−0.404	−0.395	−0.096	−0.044	−0.053	−0.010
CSF	48799602	101987231	107681216	112955078	120443466	127339954

[a]Deviations from the experimental value of 2.460 eV are also presented. The total number of configuration state functions (csf) is also listed for each active space. [b]For details of the active spaces see Figures S5−S9, SI.

with CCS, CC2, CCSD, CCSDR(T), an CCSDR(3) methods. To test the best methods as determined in section 3.3 and section 3.4 (i.e., LCC2* and empirically corrected TD-DFT in terms of accuracy and computational efficiency), eight larger conjugated BODIPYs are examined in section 3.5. Finally in section 3.6, the CASSCF wave functions are used to provide insight into the multireference character in these BODIPYs. In the conclusions, the nature of transitions in these systems is addressed and suggestions are provided on the best choice of theoretical approach for examining excitation energies for BODIPYs.

2. COMPUTATIONAL METHODS

Geometry optimizations were performed using density functional theory with the PBE0[38−40] and CAM-B3LYP[41] functionals and the cc-pVTZ[42,43] basis set in the gas phase. It has been shown previously that PBE0 is a very good functional for ground state (GS) optimization of BODIPY based compounds.[23] The excited state (ES) geometries were determined using TD-DFT with the CAM-B3LYP functional as suggested by the benchmark studies of Jacquemin et al.[44,45] "Tight" convergence criteria, i.e., maximum force = 1.5×10^{-5} au, RMS force = 1.0×10^{-5} au, max displacement = 6.0×10^{-5}, and RMS displacement = 4.0×10^{-5} were applied for both GS and ES optimizations. The grid used for numerical integration in DFT was set to "ultrafine," i.e., a pruned grid of 99 radial shells and 590 angular points per shell. Harmonic vibrational frequencies were computed at the same level of theory for both S_0 and S_1 states in order to characterize the stationary points as true minima, representing equilibrium structures on the potential energy surfaces. In order to assess the effects of the solvent environment on the optimized geometry, the GS and ES structures of **1** and **2** were reoptimized using the polarizable continuum model (IEF-PCM[46,47] and universal force field (UFF) atomic radii) with parameters for methanol (ϵ = 32.613). Not surprisingly, the solvent had no significant impact on geometries of both the S_0 and S_1 states (see Figure S1, Supporting Information (SI)). Experimentally obtained excitation energies for the BODIPY molecule (**1**) are 2.460 and 2.485 eV in cyclohexane and ethanol, respectively.[15] In agreement with experiment, the PBE0/cc-pVTZ computed excitation energy of 3.186 eV for the BODIPY molecule in the gas phase slightly decreases to 3.082 eV in methanol and to 3.042 eV in cyclohexane, i.e., no significant change in excitation energy due to solvent. While it has been shown by Chibani et al. that the corrected linear-response (cLR) and state-specific (SS) PCM solvation models are in most cases superior to the linear-response PCM (LR-PCM) results for the BODIPY molecules,[26,27] they have demonstrated that the gas phase results are, in general, close to those determined using the superior solvation models. Therefore, gas phase results will be discussed throughout the text. Symmetry was used whenever possible to simplify calculations, and this was crucially important for MRSCF computations. Nine different DFT functionals, BLYP,[48−50] PBE,[38,39] B3LYP,[51,52] PBE0, LC-BLYP,[53] LC-PBE, CAM-B3LYP, ωB97X-D,[54] and LC-ωPBE,[55−57] from generalized gradient approximations (GGA) to range-separated hybrids were used to obtain vertical transitions for 10 singlet ESs (S_1−S_{10}) using the PBE0 optimized geometries. 0−0 transition energies were also obtained for all species using the range-separated CAM-B3LYP functional as recommended by the benchmark study of Jacquemin et al.[44] The 0−0 transition energy is determined as $\Delta E^{0-0} = E^{\text{adia}} + \Delta E^{\text{ZPE}}$ where E^{adia} is the energy difference between the optimized S_1 and S_0 states and the latter is the corresponding zero point energy difference of those two states.

TD-DFT results were compared and contrasted with configuration interaction (CI) results determined using single excitations (CIS)[58] and including perturbative corrections for double excitations (CIS(D)).[59] Electron correlated equation of motion coupled-cluster with singles and doubles (EOM-CCSD)[60−63] along with Laplace transformed local coupled-cluster singles and approximate doubles (LT-DF-LCC2 abbreviated LCC2* hereafter)[64,65] and symmetry adapted cluster/configuration interaction (SAC-CI)[66] methods were utilized for all studied structures. The efficient direct algorithm was utilized for all the SAC-CI computations which corresponds to the conventional SAC-CI with NounlinkedSelection keywords. To account for the effect of the electron correlation and also to understand the convergence of the CC methods better, coupled-cluster CCS, CC2, LR-CCSD, CCSDR(T), and CCSDR(3) computations were performed for the vertical excitation energies of the smallest BODIPYs, i.e., **1**−$\mathbf{5}_{\mathrm{H}}$. Multireference complete active space self-consistent field (CASSCF)[67] [and complete active space second order perturbation (CASPT2)][68] computations were accomplished for all [most] systems. The CASPT2 computations utilized the internally contracted RS2C program.[68] The CASSCF wave functions were constructed by using equal weights of the S_0 and S_1 states. The CASPT2 computations used an IPEA shift, which is a correction to the zero order Hamiltonian, of 0.3.[69] To investigate the effect of altering active spaces on the vertical transition energies, six different active spaces were considered starting from including just the highest occupied molecular orbital (HOMO) and the lowest unoccupied molecular orbital (LUMO) (CAS[2,2]) to including all of the π electrons and the nitrogen lone pair (CAS[12,11]) for the first compound (Table 1). Not surprisingly, selecting an appropriate active space has a critical impact on the absolute value of the CASSCF transition energy. However, the effect of enlarging the active space was

DOI: 10.1021/ct500775r
J. Chem. Theory Comput. 2015, 11, 2619−2632

not as significant for the CASPT2 energies. Since enlarging the active space has a significant impact on the CASSCF transition energy, all π electrons and lone pairs were included in the active space, whenever possible, as the least amount of error was observed for that case. Also the effect of enlarging the basis set from cc-pVXZ[42] to aug-cc-pVXZ[43,70] (X = D and T) on the excitation energy was investigated and the corresponding results are provided in Table 2. Increasing the size of the basis from cc-pVDZ to cc-pVTZ does not have a major impact on accuracy nor does including diffuse functions. Overall, cc-pVDZ seems to be a suitable and cost efficient basis set and was utilized for CASSCF/CASPT2 computations throughout this work unless otherwise stated.

Table 2. CASSCF/CASPT2(12,11) Vertical Excitation Energies (eV) of 1 along with Deviations from the Experimental Value of 2.460 eV Using (aug)-cc-pVXZ (X = D, T) Basis Sets in the Gas Phase[a]

CASSCF	cc-pVDZ	cc-pVTZ	aug-cc-pVDZ	aug-cc-pVTZ
energy	2.857	2.841	2.820	2.834
deviation	+0.383	+0.369	+0.360	+0.374
CASPT2	cc-pVDZ	cc-pVTZ	aug-cc-pVDZ	aug-cc-pVTZ
energy	2.539	2.452	2.441	2.415
deviation	+0.078	−0.010	−0.021	−0.045
CSF	17629314	127339954	57729570	127570949

[a]The total number of configuration state functions (CSF) is also listed for each basis set.

Very recently proposed charge transfer indices, q^{CT} (amount of the transferred charge) and d^{CT} (CT distance based on the hole−electron distance), by Ciofini and co-workers,[71,72] are also reported for all compounds. Moreover, to predict the reliability of using a single-reference based method, three different diagnostic tests were carried out by performing CCSD,[73−76] CCSD(T),[77] and CASSCF computations for all of the systems. It is worthwhile mentioning that all of these tests refer to the multireference character of the ground state not the excited state. First, the T_1 diagnostic test of Lee and Taylor, which is based on the norm of the vector of single-excitation amplitudes from CCSD in a closed shell system,[78] was utilized. If the T_1 value is smaller than 0.02, the system is considered to be dominated by a single reference, but if it is larger than 0.02, the system is considered to have (most likely) multireference character. Second, the %TAE[T] diagnostic test related to percent atomization energy due to triples was computed for all of the BODIPY species as

$$\%\mathrm{TAE[T]} = 100\left(\frac{\mathrm{ae[CCSD(T) - CCSD]}}{\mathrm{ae[CCSD(T)]}}\right) \quad (1)$$

where ae is the atomization energy of the system under consideration using either CCSD or CCSD(T) methods.[79] If %TAE[T] is smaller than 2%, the system is considered as a single-reference system; otherwise, it is considered as a multireference system. Finally, the M diagnostic test is computed for all BODIPY systems.[80] For a closed shell system in its equilibrium geometry, M is defined as

$$M = \frac{1}{2}(2 - [n(\mathrm{MCDONO}) - n(\mathrm{MCUNO})]) \quad (2)$$

where n(j) is a natural orbital occupation number computed as the eigenvalue of the first order density matrix of a CASSCF wave function. More specifically, n(MCDONO) and n(MCUNO) are respectively the natural occupation numbers of the most correlated doubly occupied natural orbital and the most correlating unoccupied natural orbital. Based on the work of Truhlar and co-workers who introduced the M parameter,[80] if it is larger than 0.04, then the system is considered as a multireference system; otherwise, it is considered to be a single-reference system.

All DFT, TD-DFT, CIS, CIS(D) SAC-CI, CCSD, CCSD-(T), and EOM-CCSD computations were performed using Gaussian 09.[81] LCC2* and MRSCF computations were accomplished using the 2010 and 2012 Molpro packages.[82] Also, coupled-cluster CCS, CC2, LR-CCSD, CCSDR(T), and CCSDR(3) excitation energies were computed using the DALTON program package.[83]

3. RESULTS AND DISCUSSION

A set of 17 BODIPY based structures was chosen for examination starting from the head of the family, i.e., BODIPY itself (**1**); see Figure 1 for all structures considered. Substituting the carbon atom of BODIPY in the meso position with nitrogen produces aza-BODIPY (**2**) which provides a promising building block for the generation of new near IR emitting chromophores.[84] The carbon substituted boron 2-(2-pyridyl)imidazole (BOPIM) complex (**3**) and BOPIM itself (**4**) are next; **3** has not yet been synthesized. Despite the fact that **1** and **3** along with **2** and **4** are isomers and all four of them are isoelectronic, we will see later they have very different photophysical properties. The strongly fluorescent biimidazol-2-yl-BF2 complex (**5**) and its hydrogenated form ($\mathbf{5}_H$) have a common feature with **3** and **4**; all have a central five-membered ring rather than a six-membered one as in the other compounds. Difluoro-boron-triaza-anthracene (**6**), BF_2 linked green fluorescent protein (GFP) chromophore analogs (**7**) and (**9**), and the BF_2 linked GFP chromophore itself (**8**) are also in the set of structures considered in this work; for the benchmark study on the GFP chromophore itself see the work of Uppsten and Durbeej.[85] In addition, substituted complexes of **1** and **6** were chosen to show the impact of substitution of both electron donor (amino (**10**) and thio (**14**)) and acceptor (cyano (**11** and **12**)) groups on the photophysical properties of these compounds. To investigate the effect of replacing the fluorine atoms and fusing different carbocyclic rings, compounds **13**, **15**, and **16** were chosen to be examined.

3.1. S_0 and S_1 Optimized Geometries. The PBE0 and CAM-B3LYP functionals were used for the S_0 GS (Figures S2 and S3, SI) and CAM-B3LYP for the S_1 ES (Figure S4, SI) geometry optimizations. The optimized CAM-B3LYP geometry for the S_0 state is very similar to the parameter free PBE0 one with only 0.001−0.003 Å bond length differences for **1**. The largest deviation from the X-ray structure for **1**[15] relates to the B−N bond for which both PBE0 and CAM-B3LYP exhibit a 0.021 and 0.020 Å elongation, respectively. This can most likely be attributed to the fact that experimental geometry is obtained in the solid state, but our optimizations are done in vacuum. Therefore, relatively speaking, both PBE0 and CAM-B3LYP geometries are in very good agreement with the available experimental data. Hence for the sake of consistency, PBE0 geometries for the GS are used for the rest of the computations. Despite differences in the size of their rings or substituents, the GS of all structures, excluding the BF_2 groups, is planar and this is most likely due to high degrees of conjugation and resonance. Expectedly, bond lengths and relative positions of the

DOI: 10.1021/ct500775r
J. Chem. Theory Comput. 2015, 11, 2619−2632

Table 3. Vertical Excitation Energies (eV) Using Nine Different Functionals and the cc-pVTZ Basis Set in the Gas Phase[a]

type	GGA		HGGA		RSH					
functional	BLYP	PBE	B3LYP	PBE0	LC-BLYP	LC-PBE	CAM-B3LYP	ωB97X-D	LC-ωPBE	exp
1	3.006	3.020	3.154	3.186	3.073	3.084	3.145	3.147	3.077	2.460[15] (2.407)
2	2.732	2.743	2.889	2.916	2.714	2.723	2.853	2.852	2.733	2.252[b] (−)
3	2.803	2.824	3.223	3.337	3.930	3.956	3.649	3.690	3.893	3.259[b] (−)
4	2.837	2.854	3.280	3.397	4.104	4.128	3.756	3.801	4.051	4.175[86] (3.679)
$\mathbf{5}_H$	4.078	4.109	4.285	4.366	4.726	4.764	4.489	4.497	4.686	4.138[b] (−)
5	3.664	3.687	3.884	3.961	4.348	4.384	4.101	4.122	4.318	3.712[87] (3.289)
6	3.254	3.273	3.598	3.680	3.942	3.964	3.808	3.830	3.907	3.125[88] (3.112)
7	2.993	3.007	3.122	3.161	3.230	3.239	3.180	3.178	3.204	2.583[89] (2.525)
8	3.020	3.032	3.262	3.328	3.674	3.687	3.470	3.486	3.622	2.995[90] (2.605)
9	2.851	2.865	2.953	2.979	2.946	2.953	2.959	2.953	2.932	2.479[b] (−)
10	3.262	3.282	3.445	3.504	3.697	3.719	3.583	3.596	3.670	2.963[91] (2.678)
11	2.423	2.425	2.615	2.646	2.587	2.594	2.638	2.636	2.589	2.109[92] (2.026)
12	2.813	2.827	3.170	3.254	3.608	3.625	3.430	3.452	3.565	2.755[93] (2.719)
13	2.755	2.770	2.904	2.933	2.896	2.905	2.925	2.925	2.886	2.412[94] (2.322)
14	2.954	2.968	3.101	3.137	3.111	3.125	3.132	3.136	3.106	2.353[95] (2.300)
15	2.725	2.726	2.920	2.955	2.941	2.950	2.962	2.968	2.932	2.422[96] (2.317)
16	2.718	2.724	2.839	2.867	2.819	2.830	2.857	2.866	2.820	2.317[96] (2.214)
mean AE	0.364	0.367	0.470	0.513	0.587	0.605	0.545	0.556	0.572	
mean AE[c]	0.303	0.308	0.444	0.492	0.624	0.635	0.553	0.563	0.600	
max AE	1.338	1.321	0.895	0.778	0.817	0.839	0.779	0.783	0.810	
min AE	0.025	0.025	0.036	0.008	0.071	0.047	0.184	0.206	0.125	
SD[c]	0.364	0.371	0.499	0.541	0.652	0.669	0.574	0.593	0.632	
R^{2c}	0.793	0.797	0.905	0.923	0.963	0.964	0.961	0.961	0.966	

[a]Experimental values (exp, including fluorescence in parentheses) are tabulated for comparison. Absolute errors (AE) (mean AE, max AE, and min AE), standard deviation (SD), and linear determination coefficient (R^2) are also shown for each functional. All of the transitions correspond to HOMO → LUMO ($\pi \rightarrow \pi^*$). Experiments carried out in different solvents but, when determined, solvent-induced shifts are small. [b]CASPT2 value was used. [c]Determined excluding compound **4** that has the max AE for GGA and HGGA functionals.

substituents to the plane of the molecule change by going from the S_0 to S_1 state. It is also worthwhile mentioning that the C═O, C−OH, and C−NH(CH_3) bond elongations are the most important geometrical impact of the electronic excitation (Figures S3 and S4, SI). Moreover, in some molecules such as in **1** and **2**, the BF_2 unit goes out of the plane in the ES and therefore reduces the symmetry from C_{2v} to C_s (Figure S4, SI).

3.2. TD-DFT Vertical Excitations versus 0−0 Transitions (ΔE^{0-0}). TD-DFT absorption energies (eV) for all 17 compounds are presented in Table 3; all excitations correspond to $\pi \rightarrow \pi^*$ transitions. Despite the differences between structures and substituents, there is a hypsochromic shift for the TD-DFT absorption energies with respect to the experimental (CASPT2 for **2**, **3**, $\mathbf{5}_H$, and **9**) data for all of the functionals considered.

Table 3 also presents statistical analyses of the TD-DFT results, i.e., mean absolute error (mean AE), maximum absolute error (max AE), and minimum absolute error (min AE). All functionals, regardless of family, have mean AEs greater than 0.36 eV; this is outside the range of deviation (0.1−0.3 eV) typically reported for TD-DFT methods even if one accounts for the modest shift due to solvation, e.g., ∼ 0.1 eV for compound **1**; see section 2. The mean AE is slightly reduced for GGA and HGGA functionals if we exclude compound **4**, and thus most statistical analyses are reported excluding this compound. Surprisingly, pure GGA BLYP and PBE functionals seem to be the best TD-DFT functionals in terms of the absolute values and deviations from the experiment. The agreement is most likely due to cancellation of errors. This phenomenon is reported previously in the benchmark study of Walczak et al. on retinal analogues.[97] All range-separated hybrid functionals provide poorer accuracies compared to GGA and HGGA functionals and are rather close to each other. However, based on mean AE, CAM-B3LYP works slightly better. Although HGGA B3LYP and PBE0 functionals are slightly better than the RSH functionals in terms of the mean AEs, they provide very poor transition energies overall which are in some cases ∼0.8−0.9 eV blue-shifted. The standard deviation (SD) confirms the deficiency of HGGA functionals compared to pure hybrids. However, based on values of the linear coefficients of determination (R^2), range-separated hybrid methods are predictive if scaled and shifted appropriately and therefore can provide consistent predictive results (see Table S2, SI for linear fitting coefficients of all methods). These results are in agreement with previous extensive benchmarks of the BODIPY monomers and dimers[30] and aza-BODIPYs[23] performed by Jacquemin and co-workers. In their publications, the M06-2X functional was recommended for the BODIPY molecules along with accounting for state-specific solvation and ZPE corrections. On the other hand, one can see similar statistical parameters for the B3LYP, PBE0, CAM-B3LYP, and ωB97X-D functionals used in both the present and Jacquemin's studies even though, except for five molecules, the sets of systems examined are different.[30] Finally, the benchmark of Jacquemin et al., with an almost identical set of functionals, on the vertical excitation energies of relatively large aza-BODIPYs provided another set of interesting results. They proposed the BMK//PBE0 quick recipe for large systems, but they also emphasized the necessity of geometric relaxation of the excited state and vibrational corrections whenever it is computationally possible.

DOI: 10.1021/ct500775r
J. Chem. Theory Comput. 2015, 11, 2619−2632

The impact of ring size and substituent is also apparent from Table 3. For structures **3**−**5**, which have a five-membered ring in the middle instead of six, all TD-DFT functionals are able to predict the significant blue shift with respect to **1**. The effect of substituents, which play a large role in shifting the wavelength of the maximum absorption, are also well-predicted by most of the functionals. For the following comparison with experiment, the LC-ωPBE functional is used since it shows the highest R^2 value among all (although the value of R^2 is probably not statistically different from the other range-separated hybrids); see Figure 2; LCC2* results will be discussed in section 3.4.

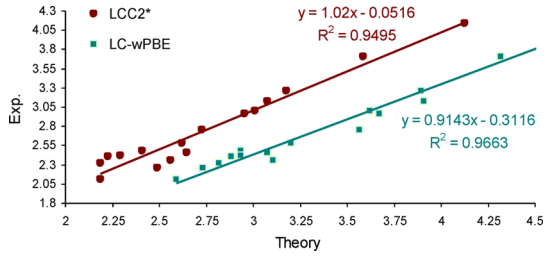

Figure 2. Comparison between LCC2* and LC-ωPBE computed vertical excitation energies and experiment ("Exp.") for all the studied species except **4**. The cc-pVTZ basis set is used for both methods.

The electron donating aminomethyl group in **10** decreases the experimental (LC-ωPBE) maximum absorption of **1** (nm) by as much as 86 (65) while the cyano (**11**) and thio (**14**) groups increase this value 84 (76) and 23 (−3.8), respectively. Attaching five- and six-membered rings to **1** results in formation of **15** and **16** which also show a bathochromic shift for the maximum absorption. For **15** and **16**, LC-ωPBE can successfully predict the direction and magnitude of this shift (experimental (LC-ωPBE) shifts from **1** in nanometers are 7.9 (19.9) and 31.1 (36.7), respectively). Overall, it seems that TD-DFT is able to reproduce the trends whenever the shift due to substitution is quite high, and this is one of the strengths of the TD-DFT methods. However, when the shift is small, TD-DFT methods have problems determining the correct shift direction.

To assess the impact of the vertical approximation on the theoretically determined absorption maxima, ΔE^{0-0} energies were obtained using the range-separated hybrid CAM-B3LYP method, the RSH with the smallest mean AE. It has been shown that this approach can provide more reliable and accurate data rather than raw vertical transition energies.[25−27,35,44,98−100] Results of these calculations along with the regular vertical absorption and emission energies and oscillator strengths are provided in Table 4. Theoretical 0−0 energies are compared to the experimental energies at the absorption maximum rather than the absorption and emission crossing point as suggested previously;[30,35,44,99] this should not strongly impact the statistical analysis. One cannot see a major improvement in the agreement with the experimental measurements for the 0−0 computations; i.e., the mean AE and SD are improved modestly while the linear coefficient of determination is significantly decreased (mean AE = 0.379, max AE = 0.804 eV, min AE = 0.022 eV, SD = 0.397 eV, and R^2 = 0.862). However, this method is certainly capable of removing some of the error cancellations that exist in the vertical approach. Overall, the least amount of improvement is obtained for **1**, **2**, and **15**, probably due to the stiffness of their structures. Their absorption values are 0.152, 0.157, and 0.152 eV, respectively, lower than their adiabatic vertical excitation energies; i.e., they still overestimate the experiment by respectively 0.533, 0.444, and 0.521 eV. Results become slightly better in the cases of **3** and $\mathbf{5}_{\mathrm{H}}$ (0.367 and 0.455 eV shifts, respectively).

Comparing fluorescence energies with the experimentally available ones for our systems show a similar range of errors; see Table 3 and Table 4. For fluorescence, mean AE = 0.479 eV and SD = 0.678 eV. The R^2 value of 0.924 is slightly better than the corresponding value for the 0−0 energies but worse than that for the adiabatic absorption energies (Table 3). However, the CAM-B3LYP functional seems to predict the Stokes shift (the difference between the absorption and emission energies) quite reasonably, for example, within ∼0.05 eV for compounds **5**, **13**, **15**, and **16** but with approximately 0.2 eV difference with experiment for compounds **6**, **7**, **12**, and **14** (Table 4).

Table 4. CAM-B3LYP/cc-pVTZ Computed Maximum Absorption and Fluorescence Energies (ΔE^{abs} and ΔE^{flu} (eV), respectively) and Their Oscillator Strengths (f^{abs} and f^{flu}) along with the 0−0 Transition Energies (ΔE^{0-0}) in the Gas Phase[a]

species	state	ΔE^{abs}	f^{abs}	ΔE^{0-0}	ΔE^{flu}	f^{flu}	shift
1	B_2	3.145	0.507	2.993	3.013	0.430	0.152 (0.053)
2	B_2	2.853	0.462	2.696	2.722	0.387	0.157 (−)
3	A′	3.649	0.236	3.282	3.055	0.129	0.367 (−)
4	A′	3.756	0.233	3.371	3.145	0.150	0.385 (0.496)
$\mathbf{5}_H$	A′	4.489	0.382	4.034	3.815	0.369	0.455 (−)
5	A′	4.101	0.485	3.699	3.473	0.469	0.402 (0.423)
6	A″	3.808	0.399	3.552	3.579	0.362	0.256 (0.013)
7	A	3.180	0.668	2.972	2.938	0.611	0.208 (0.058)
8	A′	3.470	0.685	3.244	3.120	0.646	0.226 (0.390)
9	A′	2.959	0.657	2.787	2.748	0.597	0.172 (−)
10	A	3.583	0.424	3.346	3.223	0.342	0.237 (0.285)
11	B	2.638	0.541	2.496	2.532	0.482	0.142 (0.083)
12	A″	3.430	0.356	3.213	3.085	0.219	0.217 (0.036)
13	A″	2.925	0.567	2.835	2.790	0.527	0.090 (0.090)
14	A	3.132	0.432	2.874	2.871	0.368	0.258 (0.053)
15	A	2.962	0.573	2.806	2.869	0.509	0.156 (0.105)
16	A″	2.857	0.635	2.699	2.769	0.582	0.158 (0.103)

[a]Stokes shifts (shift) for CAM-B3LYP as well as experiment (in parentheses) are also provided in eV. See Table 3 for the experimental values.

DOI: 10.1021/ct500775r
J. Chem. Theory Comput. 2015, 11, 2619−2632

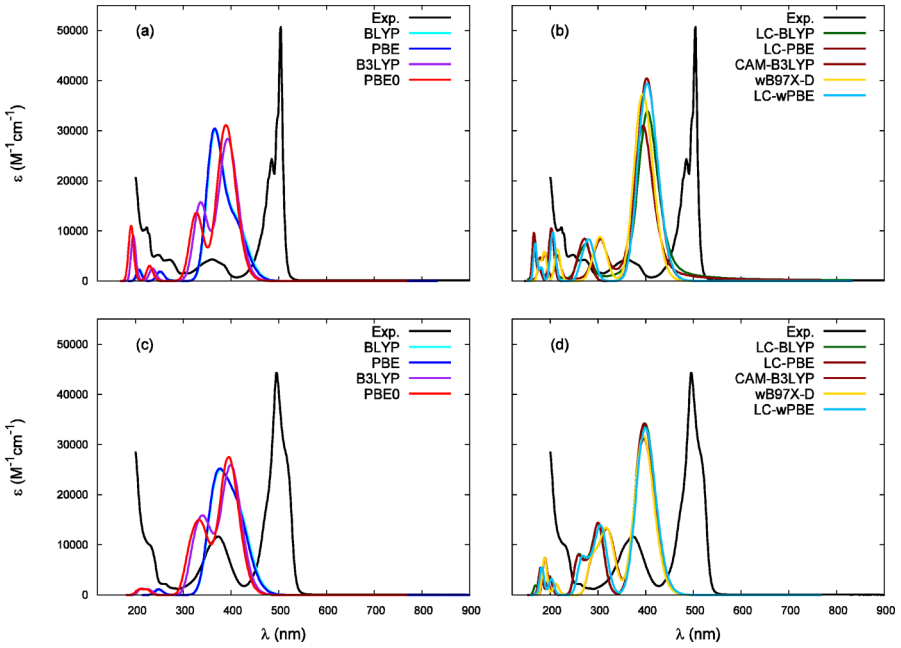

Figure 3. TD-DFT computed absorption spectra of **1** (a and b) and **14** (c and d) using nine different functionals in the gas phase. Experimental spectra ("Exp.") are obtained in cyclohexane solution.[91]

Figure 3 compares and contrasts the spectral shapes for **1** and **14** obtained using all nine TD-DFT functionals with the experimental ones obtained in cyclohexane solutions;[91] these are chosen as examples for which we had access to the experimental spectra. For simulation of the spectral shape, the AOMix program[101,102] was used in which the default value of 3000.0 cm^{-1} for the bandwidth was utilized. In terms of the positions of the peaks, all TD-DFT methods tend to overestimate the absorption energies for these BODIPYs. The shift between the TD-DFT and experimental results for both the peak at higher wavelength (located at approximately 500 nm in the spectra) and the one at the lower wavelength (at ∼350−370 nm in the spectra) are nearly the same and approximately 100 nm for all functionals. The simulated intensity of the lowest energy peaks for both **1** and **14** are also a bit lower than the obtained experimental ones specifically for the CAM-B3LYP functional in the case of compound **1** and also the GGA functionals in both cases; the agreement could be modestly improved by narrowing the simulated bandwidth. Overall, based on the relative peak positions and intensities, LC-ωPBE and ωB97X-D seem to be reasonably reliable functionals for simulating the absorption spectra of these compounds and GGA and HGGA ones seem to be among the worst.

3.3. Charge Transfer Parameters and Electron Density Difference Plots. Depending on the nature of the excitation (valence, CT, and so on) or whether (or not) there are push−pull substituents in the system of interest, different TD-DFT methods should be applied to determine accurately the excitation energies. More important is to determine measures to assess the nature of the transition. For example, the range-separated hybrid methods, such as CAM-B3LYP, have been designed to correct some of the deficiencies of their hybrid ancestors with respect to long-range excitations. Table 5 provides the computed CT parameters for all species using the range-separated hybrid CAM-B3LYP functional in the gas phase. Electron density difference plots are also useful for assessing the nature of the excitation and are given for all species in Figure S5, SI. The least amount of transferred charge (q^{CT}) and the CT distance (d^{CT}) correspond to the heads of the family, i.e., **1** and **2** as well as the six-membered analogue of **2**, i.e., **6**. The order for the smallest CT dipole moment is also the same (Table 5). On the other hand, the five-membered rings (**3**−**5**) have the highest values for these indices (the BF_2 linked GFP chromophore (**8**) with a six-membered ring also has significant values for these indices). EDD plots also confirm this finding as the density difference between the GS and ES is delocalized over molecules **3**−**5** compared to the rest of the systems where the EDD is only distributed on the "upper" part of them (as drawn in Figure 1, i.e., excluding the BF_2 unit and nitrogens attached to them). Examples of EDD plots for **2** and

Table 5. Computed Charge Transfer (CT) Parameters (q^{CT} and d^{CT}), along with Ground State/Excited State (μ^{grd}/μ^{exc}) and CT (μ^{CT}) Dipole Moments (in Debye) at the CAM-B3LYP/cc-pVTZ Level of Theory

species	q^{CT}	d^{CT}	μ^{grd}	μ^{exc}	μ^{CT}
1	0.351	0.232	4.327	4.116	0.391
2	0.340	0.057	2.303	2.327	0.092
3	0.609	1.772	5.610	4.691	5.182
4	0.634	1.913	5.074	2.711	5.824
$\mathbf{5}_H$	0.460	1.072	5.751	5.043	2.369
5	0.486	1.154	5.713	4.545	2.692
6	0.427	0.091	2.020	2.493	0.187
7	0.382	0.792	2.315	1.235	1.454
8	0.437	1.594	2.822	1.502	3.343
9	0.354	0.866	3.783	2.804	1.471
10	0.441	0.824	7.770	5.717	1.745
11	0.358	0.638	0.234	1.330	1.098
12	0.460	0.636	3.001	3.777	1.405
13	0.383	0.441	3.322	2.605	0.810
14	0.370	0.554	5.480	3.495	0.985
15	0.396	0.385	4.412	3.866	0.733
16	0.382	0.444	3.379	2.719	0.816

DOI: 10.1021/ct500775r
J. Chem. Theory Comput. 2015, 11, 2619−2632

4, i.e., members of the two types of excitations observed, are shown in Figure 4. For EDD plots of all compounds see Figure S5, SI. Participation of the functional groups in the transitions is also evident, for example, see compound **8** that shows values of 0.437 *e*, 1.594 Å, and 3.343 D for q^{CT}, d^{CT}, and μ^{CT}, respectively. The phenomenon can be observed to some extent in other substituted species such as **7**, **9**, **10**, and **12**.

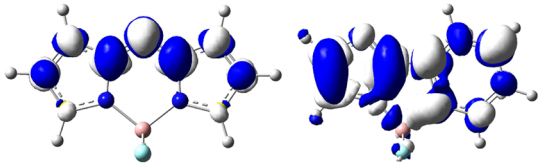

Figure 4. Electron density difference (EDD) between the excited state and ground state of **2** and **4** with isovalue of 0.002 au calculated at the CAM-B3LYP/cc-pVTZ level of theory. White and blue regions correspond to density increase and decrease, respectively, upon electron excitation.

From the CT indices, although CT is somewhat significant in compounds **3**−**5**, it is most likely not large enough to be solely responsible for the problems of TD-DFT inaccurately reproducing the absolute vertical excitation energies for these systems nor does it explain problems for the other compounds where the CT indices have lower values. Importantly, compounds **1** and **2**, for which TD-DFT also exhibits large deviations from experiment, show negligible CT characteristics. This agrees with the seminal works of Tozer[103] and Dreuw and Head-Gordon[104] that CT (in most cases) is reflected in an underestimations of the TD-DFT excitation energies (rather than the overestimation observed here). We will discuss the reasons behind the TD-DFT failures for these compounds at the end of the next section where CI vectors from CASSCF computations are considered.

3.4. Benchmarking ab Initio and MRSCF Methods. All ab initio and multireference results using both cc-pVDZ and cc-pVTZ basis sets are depicted in Table 6 along with the corresponding statistical analyses. First of all, enlarging the basis set from cc-pVDZ to cc-pVTZ shifts the energy less than 0.1 eV (red shift) for all methods, except 0.204 eV for LCC2* of **5** (see also Table S1, SI, for EOM-CCSD, CASSCF, and CASPT2 results for **1**−**5** with the cc-pVTZ basis set). The size consistent configuration interaction with singles only (CIS) method shows the poorest agreement with experiment among all of the methods applied in this study (even poorer than TD-HF) with the largest mean AE, max AE, and SD (Table 6). On the other hand, although TD-HF exhibits a smaller mean AE than CIS, its R^2 value is also (slightly) smaller than corresponding CIS results with values of 0.912 (0.915) for cc-pVDZ (cc-pVTZ) basis sets. However, the TD-HF and CIS results demonstrate that it is possible to get rough estimates of excitation energies for extremely large BODIPY systems, for which electron correlated methods are not applicable due to system size, by correcting the results of either TD-HF or CIS methods (See Table S2, SI for linear fitting coefficients of all methods).

Applying the perturbative doubles (D) correction significantly improves the CIS results where, for cc-pVDZ (cc-

Table 6. Vertical Excitation Energies Using Different ab Initio Methods and the cc-pVDZ (DZ) and the cc-pVTZ (TZ, except EOM-CCSD, SAC-CI, CASSCF[b], and CASPT2[b] methods) Basis Sets in the Gas Phase[a]

method	TD-HF		CIS		CIS(D)		LCC2*		EOM-CCSD	SAC-CI	CASSCF	CASPT2
basis	DZ	TZ	DZ	TZ	DZ	TZ	DZ	TZ	DZ	DZ	DZ	DZ
1	3.266	3.206	3.578	3.519	3.021	2.968	2.679	2.647	2.973	2.657	2.829	2.538
2	2.846	2.762	3.225	3.146	2.846	2.788	2.531	2.492	2.725	2.425	2.565	2.344
3	4.225	4.159	4.471	4.407	3.744	3.655	3.269	3.176	3.777	3.310	3.730	3.129
4	4.378	4.311	4.622	4.558	3.876	3.776	3.399	3.308	3.936	3.464	3.933	3.278
$\mathbf{5}_H$	4.898	4.898	5.255	5.167	4.713	4.564	4.283	4.125	4.751	4.331	4.933	4.104
5	4.650	4.550	4.902	4.806	4.294	4.136	3.791	3.587	4.393	3.764	4.704	3.726
6	4.398	4.355	4.619	4.577	3.607	3.555	3.149	3.074	3.747	3.177	3.904	2.821
7	3.535	3.472	3.823	3.762	3.090	3.004	2.653	2.623	3.206	2.424	3.510	–
8	4.033	3.979	4.293	4.242	3.555	3.458	3.011	3.011	3.697	2.959	4.313	3.142
9	3.184	3.099	3.526	3.446	2.921	2.822	2.468	2.408	3.029	2.299	3.277	2.479
10	3.998	3.922	4.232	4.160	3.537	3.440	3.058	2.953	3.579	2.967	3.627	3.055
11	2.733	2.682	3.072	3.023	2.640	2.579	2.242	2.187	2.626	2.015	2.998	1.957
12	4.047	3.990	4.250	4.193	3.254	3.181	2.816	2.726	3.395	2.700	3.485	2.693
13	3.083	3.043	3.380	3.343	2.783	2.735	2.278	2.226	2.815	1.966	3.647	–
14	3.328	3.261	3.614	3.548	2.996	2.921	2.631	2.560	3.002	2.342	2.924	2.448
15	3.153	3.110	3.447	3.407	2.825	2.773	2.339	2.294	2.846	2.043	2.887	–
16	3.015	2.967	3.314	3.269	2.742	2.692	2.216	2.187	2.746	1.932	3.457	–
mean AE	0.839	0.780	1.124	1.061	0.500	0.431	0.148	0.145	0.542	0.187	0.747	0.161
mean AE[c]	0.879	0.820	1.167	1.104	0.513	0.434	0.109	0.100	0.561	0.154	0.778	0.100
max AE	1.292	1.235	1.495	1.438	0.643	0.568	0.776	0.867	0.702	0.711	1.318	0.897
min AE	0.594	0.510	0.963	0.894	0.371	0.323	0.010	0.010	0.403	0.004	0.313	0.014
SD[c]	0.886	0.830	1.152	1.090	0.509	0.428	0.135	0.119	0.558	0.206	0.831	0.126
R^{2c}	0.912	0.915	0.940	0.937	0.983	0.985	0.954	0.949	0.983	0.933	0.802	0.954

[a]Mean AE, max AE, min AE, SD, and R^2 are also listed for each method. See Table 3 for the experimental values. [b]For details of the computations see SI. [c]Determined excluding compound **4**.

DOI: 10.1021/ct500775r
J. Chem. Theory Comput. 2015, 11, 2619−2632

Table 7. Computed Coupled Cluster Vertical Excitation Energies (eV) for Compounds 1−5_H Using the cc-pVDZ Basis Set[a]

species	CCS	CC2	CCSD	CCSDR(T)	CCSDR(3)
1	3.578 (+1.118)	3.017 (+0.557)	2.973 (+0.513)	2.380 (−0.080)	2.895 (+0.435)
2	3.225 (+0.881)	2.800 (+0.456)	2.725 (+0.381)	2.074 (−0.270)	2.658 (+0.314)
3	4.471 (+1.212)	3.586 (+0.327)	3.777 (+0.527)	3.155 (−0.095)	3.624 (+0.495)
4	4.621 (+1.343)	3.713 (+0.435)	3.936 (+0.660)	3.297 (+0.019)	3.770 (+0.492)
5_H	5.255 (+1.117)	4.609 (+0.471)	4.751 (+0.613)	4.176 (+0.038)	4.628 (+0.390)

[a]Deviations from experiment (CASPT2 for compounds **2**−5_H) are also given in parentheses.

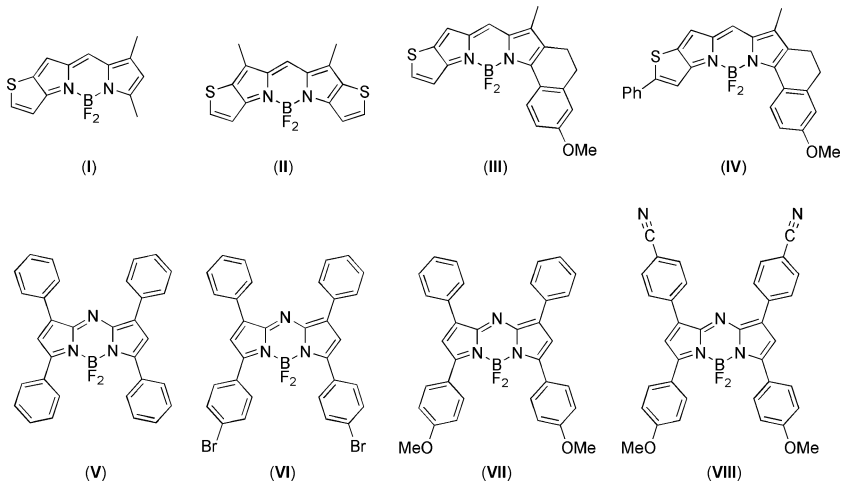

Figure 5. Conjugated BODIPYs (**I**−**IV**) and aza-BODIPYs (**V**−**VIII**) studied in this work.

pVTZ), the mean AE (eV) decreases from 1.167 (1.104) to 0.513 (0.434) and the SD from 1.152 (1.090) to 0.509 (0.428), and also R^2 has the largest value among all of the wave function based (and TD-DFT) methods. The smallest computed shift (eV) toward the red region as compared to the experimental measurements is found for compound **2**, 0.379 (0.368), and the most for compounds **12** and **6**, 0.996 (1.012) and 1.012 (1.022), respectively, using cc-pVDZ (cc-pVTZ) basis sets (Table 6). These results are in line with the work of Grimme and Neese in which the importance of perturbative doubles corrections (D) is emphasized for developing the double hybrid methods.[105]

By going from CIS(D) to the local coupled cluster second order LCC2* method, one can see another improvement in the agreement (due to an approximately 0.3−0.5 eV red shift for each compound) and the results are indeed closest to the highly accurate and sophisticated CASPT2 method, most likely due to cancellation of errors. Of course, the LCC2* approach is more applicable for larger substituted BODIPY systems. Even though R^2 slightly decreases for the LCC2* results compared to those from CIS(D) computations, the mean AE, SD, and max AE decrease by (approximately) a factor of 3−5 (Table 6).

Coupled-cluster EOM-CCSD computations were carried out using the cc-pVDZ basis set for all species and compared to all other methods. Surprisingly, a small shift from the results determined with the CIS(D)/cc-pVDZ method was found only for compounds **1** and **2** (0.048 and 0.121 eV red shift, respectively), and the EOM-CCSD/cc-pVDZ results were poorer than CIS(D)/cc-pVDZ for all other species (Table 6). Even though it is believed that this method is the more accurate version of the LCC2* method (and also SAC-CI), except for R^2, the rest of the statistical indices suggest that the EOM-CCSD method with the small cc-pVDZ basis is not a good choice for examining the excited states of BODIPY compounds. The SAC-CI method with the cc-pVDZ basis set was also computed for all systems, and the results are presented in Table 6. The mean AE decreases from 0.561 eV for the EOM-CCSD method to 0.154 eV with SAC-CI; SD decreases from 0.558 to 0.205 eV, and R^2 slightly decreases from 0.983 to 0.933. Overall, the LCC2* and SAC-CI methods seem to be very good choices for studying excited state properties of the BODIPY systems.

To better understand the effect of electron correlation and also the convergence of the coupled-cluster methods, a series of CCS, CC2, LR-CCSD, CCSDR(T), and CCSDR(3) computations were undertaken for the smallest BODIPYs, i.e., **1**−5_H); see Table 7. There is a clear trend in the convergence going from CCS to CCSDR(T) [or CCSDR(3)]. These results highlight the extreme sensitivity of the vertical excitation energies to the differences in electron correlation between the ground and excited states. The canonical CC2 results reported in Table 7 are different than their corresponding local LCC2* results reported in Table 6 and strongly suggest that the excellent performance of LCC2* is due to the cancellation of errors (attributable to the local approximation).

Multireference CASSCF and CASPT2 computations are also undertaken for all compounds using the cc-pVDZ basis set; CASPT2 computations are not carried out for compounds **7**, **13**, **15**, and **16** that represent some of the largest molecules in the set. The related cc-pVTZ data for compounds **1**−5_H can be found in Table S1, SI. In most cases, the CASSCF vertical excitation energies are worse than CIS(D) and EOM-CCSD data. The discrepancies can be readily related to the lack of dynamic electron correlation in CASSCF and also the fact that we were not able to include all of the π electrons and the nitrogen lone pairs in the active space for the larger systems (for details of the CASSCF computations see the SI). Expectedly, CASPT2 is found to be the most reliable method

DOI: 10.1021/ct500775r
J. Chem. Theory Comput. 2015, 11, 2619−2632

Table 8. Computed Vertical Excitation Energies (eV) for the Extended BODIPYs (I–IV) and aza-BODIPYs (V–VIII)[a]

species	exp	PBE0	CAM-B3LYP	LC-ωPBE	LCC2*	LC-ωPBE$^{(corr)}$	LCC2*$^{(corr)}$
I	2.331[110]	2.801 (+0.470)	2.864 (+0.533)	2.824 (+0.493)	2.401 (+0.070)	2.270 (−0.061)	2.354 (+0.023)
II	2.206[111]	2.572 (+0.366)	2.743 (+0.537)	2.691 (+0.485)	2.253 (+0.047)	2.149 (−0.057)	2.213 (+0.007)
III	2.049[111]	2.521 (+0.472)	2.547 (+0.498)	2.544 (+0.495)	1.999 (−0.050)	2.014 (−0.035)	1.970 (−0.079)
IV	1.922[111]	2.327 (+0.405)	2.376 (+0.454)	2.392 (+0.470)	1.809 (−0.113)	1.875 (−0.047)	1.789 (−0.133)
V	1.907[112,113]	2.234 (0.327)	2.240 (0.333)	2.190 (0.283)	1.825 (−0.082)	1.691 (−0.216)	1.804 (−0.103)
VI	1.884[114]	2.170 (0.286)	2.199 (+0.315)	2.159 (+0.275)	1.737 (−0.147)	1.662 (−0.222)	1.721 (−0.163)
VII	1.802[112,113,115]	2.106 (+0.304)	2.143 (+0.341)	2.107 (−0.305)	1.608 (−0.194)	1.615 (−0.187)	1.597 (−0.205)
VIII	1.732[116]	2.005 (+0.273)	2.063 (+0.331)	2.036 (+0.304)	1.509 (−0.223)	1.550 (−0.182)	1.503 (−0.229)

[a]Deviation from experiment is shown in parentheses. For the LC-ωPBE functional and the LCC2* method the corrected values (corr) based on the correlation shown in Table S2, SI, are also given.

as the mean AE (SD) slightly improves from 0.109 eV (0.135 eV) for the LCC2* method to 0.100 eV (0.126 eV) for the CASPT2 method, both with the cc-pVDZ basis set. There are some examples of applying CASSCF and/or CASPT2 methods for studying BODIPYs in the literature,[106−108] but they have focused only on a small number of examples. For instance, Briggs et al. have reported a value of 2.62 eV for the vertical excitation energy of the BODIPY parent molecule **1** at the CASPT2/6-31G* level of theory.[106] Valiev et al. have used the extended multiconfiguration quasi-degenerate second order of perturbation theory (XMCQDPT2) and CC2 methods to examine a series of five BODIPYs.[109] The differences for their CC2 energies (overestimated by 0.42−0.59 eV) are in keeping with the present CC2 results (see Table 7); interestingly, they attribute this difference due to substantial contributions of double excitations to the excited states (>10%); see the discussion in section 3.6.

3.5. Conjugated BODIPYs and Aza-BODIPYs. To expand our study to larger conjugated molecules and also to find out the impact of enlarging the conjugation length on the accuracies of the LCC2* and TD-DFT methods, four extended BODIPYs (**I**–**IV**) and four aza-BODIPYs (**V**–**VIII**) were considered (Figure 5). Similar to our previous approach, they were first optimized with the PBE0/cc-pVTZ functional in the gas phase and then their vertical excitation energies were determined by the LCC2*/cc-pVDZ method as well as PBE0, CAM-B3LYP, and LC-ωPBE functionals using the cc-pVTZ basis set; see Table 8. As can be seen from Table 8, the error for the TD-DFT functionals is 0.273−0.537 eV and it is greater by ca. 0.1−0.2 eV for the BODIPYs compared to the aza-BODIPYs. The results determined using the PBE0 functional show the lowest absolute deviations from the experimental values for all of the BODIPYs and aza-BODIPYs considered herein except **V** and **VI**; however, the AE still exceeds ca. 0.3 eV. On the other hand, the LCC2* method shows relatively small (absolute) errors for the BODIPYs, i.e., ≤0.113 eV for the uncorrected values, but it increases for the aza-BODIPYs up to 0.223 eV possibly because of enlarging the conjugation length and decreasing of the HOMO−LUMO gap. The LC-ωPBE and LCC2* corrected values are also depicted in Table 8; this functional is used because it showed a higher correlation with experiment than the PBE0 functional. Empirical corrections seem to overcome some of the TD-DFT overestimations, and therefore it is recommended for both BODIPY and aza-BODIPY molecules. However, the LCC2* values do not show a major improvement upon empirical correction except for **I** and **II**, and hence correction is not required, nor recommended, for this method.

3.6. Multireference versus Double Transitions. To test the reliability of single reference electron correlated/uncorrelated methods applied in this study, three different diagnostic tests, i.e., T_1, %TAE[T], and M, are computed for all systems and the results are depicted in Table 9. These three diagnostic tests provide insight into the multireference character of the ground electronic state and, hence, possible difficulties in using the DFT ground state as a reference for TD-DFT. Both T_1 and %TAE[T] tests suggest that the ground states of the BODIPY molecules can be treated with coupled-cluster methods. In other words, treating BODIPY systems with these methods should lead to no significant error in the results due to the use of a single reference method. On the contrary, based on the M diagnostic test (see eq 2), all of the systems exhibit a significant amount of multireference character since all have M values larger than 0.04 electron. To further examine this matter, CASSCF CI vectors (>0.05 for at least one state) of all of the GSs and ESs of the structures studied in this work are provided in Table S3, SI. For the parent BODIPY, an active space comprised of six B_1 and five A_2 symmetry orbitals was considered (12 electrons in 11 orbitals). As can be seen from SI Table S3 for the ground state of compound **1**, the two dominant configurations $|\phi_1\rangle = |(\text{core})^2\ (5B_1)^2\ (2A_2)^2\ (6B_1)^2$

Table 9. Computed T_1, %TAE, and M Diagnostic Tests Using the cc-pVDZ Basis Set[a]

species	T_1	%TAE	M	$\|CI\|^2_{S_0}$	$\|CI\|^2_{S_1}$
1	0.014	1.47	0.114	0.812	0.592
2	0.015	1.43	0.147	0.792	0.721
3	0.013	1.41	0.100	0.824	0.744
4	0.013	1.31	0.100	0.828	0.743
$\mathbf{5}_H$	0.013	1.07	0.079	0.872	0.796
5	0.013	1.04	0.079	0.872	0.805
6	0.015	1.34	0.087	0.826	0.726
7	0.015	1.14	0.097	0.865	0.806
8	0.015	1.20	0.106	0.847	0.823
9	0.015	1.10	0.139	0.800	0.762
10	0.014	1.27	0.080	0.877	0.808
11	0.013	1.33	0.106	0.852	0.816
12	0.015	1.45	0.063	0.856	0.777
13	0.013	1.38	0.054	0.929	0.916
14	0.014	1.42	0.110	0.825	0.753
15	0.013	1.33	0.112	0.837	0.766
16	0.012	1.32	0.091	0.871	0.826

[a]The square of the dominant configuration coefficients for the ground states ($|CI|^2_{S_0}$) and first excited states ($|CI|^2_{S_1}$) are also listed using the state averaged CASSCF method and the cc-pVDZ basis set.

DOI: 10.1021/ct500775r
J. Chem. Theory Comput. 2015, 11, 2619−2632

$(7B_1)^2\ (3A_2)^2\ (4A_2)^2\ (8B_1)^0\rangle$ and $|\phi_2\rangle = |(\text{core})^2\ (5B_1)^2\ (2A_2)^2\ (6B_1)^2\ (7B_1)^2\ (3A_2)^2\ (4A_2)^0\ (8B_1)^2\rangle$ contribute 81.3% and 1.6% to the wave function (Table 9). The rest of the contributions correspond to other configurations resulting from single or double electron excitations within the active space. On the other hand, the S_1 ES of this molecule has two major configurations $|\phi_1\rangle = |(\text{core})^2\ (5B_1)^2\ (2A_2)^2\ (6B_1)^2\ (7B_1)^2\ (3A_2)^2\ (4A_2)^1\ (8B_1)^1\rangle$ and $|\phi_2\rangle = |(\text{core})^2\ (5B_1)^2\ (2A_2)^2\ (6B_1)^2\ (7B_1)^2\ (3A_2)^1(4A_2)^2\ (8B_1)^1\rangle$, which contribute 59.2% and 13.7%, respectively. However, configurations corresponding to double excitations have a contribution of 7.6%.

The same active space for compound **2**, i.e., the head of the aza-BODIPY molecules, yields 79.2% of a single dominant ("GS") contribution to the S_0 wave function which is slightly smaller than that of compound **1**. However, for the S_1 ES one can see a 72.1% single electron transition from HOMO to LUMO, a 3.5% double transition comprised of one HOMO to LUMO and one HOMO−2 to LUMO, and 1.6% double transitions from HOMO−1 to LUMO and from HOMO to LUMO+3. Compounds **3**, **4**, **6**, **9**, **12**, **14**, **15**, and **8** have somewhat similar weightings for the dominant CI eigenvector for both their S_0 and S_1 states, i.e., ∼83% and ∼75%, respectively. Compounds $\mathbf{5}_H$, **5**, 7, **10**, **11**, and **16** form another group which show slightly higher values for those eigenvectors, about 87% and 81%, respectively. In complete contrast to compounds **1** and **2**, which showed the smallest values, compound **13** exhibits the largest weightings for the dominant CI eigenvector, 92.9% and 91.2%, respectively (Table S2, SI). As discussed earlier, only one index, i.e., the *M* index, illustrates a multireference character for the ground states of the BODIPYs and the two other indices show a single-reference character for them. Therefore, one cannot attribute the TD-DFT (DFT) problem solely to the multireference nature of these dyes. On the other hand, the CI eigenvectors are suggestive that double excitations play an important role in the excited states of the BODIPY family and hence contribute to the systematic deviation of TD-DFT results from the experimental measurements. The importance of double excitations for BODIPYs has been reported previously[109] and is also in line with previous reports for cyanine dyes in which the importance of double corrections is emphasized.[37,105,117]

4. CONCLUSIONS

From a quantitative point of view, all TD-DFT functionals overestimate the experimental absorption maxima by more than 0.3 eV for all 17 species that are investigated in this work. Therefore, the use of TD-DFT is not recommended unless the results are corrected empirically in an appropriate manner (see Table S2, SI). Pure BLYP and PBE functionals show promising mean AEs, but since their R^2 values are very low (0.797 and 0.793, respectively), their use is not recommended. Based on R^2 values (>0.96), all of the range-separated hybrid functionals appear moderately superior to the hybrid GGA functionals (R^2 > 0.9); therefore, most can be used if corrected appropriately. Similar TD-DFT results for BODIPYs and aza-BODIPYs have been reported previously.[30,32]

It was found that, from both accuracy and efficiency viewpoints, the LCC2* method with the cc-pVTZ or even the cc-pVDZ basis set seems to be a very good and reliable alternative candidate to either TD-DFT or high level (computationally expensive or even intractable) multireference approaches for determining vertical excitation energies of the BODIPY systems. The SAC-CI method with the cc-pVDZ basis set can be seen as the next best alternative to LCC2* as it gives a mean AE of 0.154 eV, which is almost as accurate as the CASPT2 method with the same basis set. However, compared to CASPT2, LCC2* and SAC-CI methods have the advantage of applicability for large substituted BODIPY systems. Therefore, the authors highly recommend using these methods for the study of BODIPYs.

Vertical excitation energies of the extended BODIPYs and aza-BODIPYs were also computed using the best-performing methods, i.e., LCC2*, PBE0, CAM-B3LYP, and LC-ωPBE methods; see section 3.5. Absolute errors up to +0.495 eV were found for the LC-ωPBE method, and the maximum error was reduced to +0.222 eV by empirical correction. Also, the LCC2* method showed a very good performance for both BODIPYs (AE $\leq$ 0.113 eV) and aza-BODIPYs (AE $\leq$ 0.223 eV). Importantly, empirical correction is not required, nor recommended, for this method.

The obtained CT parameters and EDD plots demonstrate that compounds **3**−**5** exhibit CT characteristics; however, not all of the studied species exhibit significant CT (see Table 5). The lack of significant CT is also suggested because there are not significant improvements in absolute performance when moving from GGA and HGGA functionals to range-separated ones. However, this may have been anticipated as problems with CT normally manifest themselves in an underestimation of the TD-DFT excitation energies,[103,104] while in the present work the use of GGA and HGGA functionals leads to a significant overestimation of the vertical excitation energies. Therefore, the problems with the predictions of TD-DFT, i.e., mean AE $\gtrsim$ 0.3−0.6 eV, cannot be attributed to the CT issue.

From the CASSCF computations, it was found that the major problem in these compounds, and, in particular, for the heads of the family, i.e., compounds **1** and **2**, arises because of the multireference nature of the transitions. For instance, the dominant CSF for the first excited state corresponding to HOMO to LUMO excitation contributed 59.2% for compound **1** and 72.1% for compound **2**. Similarly, the contributions belonging to double excitations, which in some cases make moderate 5−10% contributions (see Table S3, SI), cannot be captured by TD-DFT.

This study hopes to encourage future complementary ab initio and TD-DFT benchmarks on these problematic chromophores. Importantly, the results presented and BODIPYs in general can serve as excellent test cases for the development of new functionals and methods for TD-DFT.

■ ASSOCIATED CONTENT

Supporting Information

The cc-pVTZ calculated vertical excitation energies using EOM-CCSD, CASSCF, and CASPT2 methods (Table S1), linear fitting coefficients of all ab initio and TD-DFT methods considered (Table S2), CASSCF/cc-pVDZ computed CI vectors for all studied structures (Table S3), PBE0/cc-pVTZ computed gas phase XYZ coordinates for all GS structures (Table S4), CAM-B3LYP/cc-pVTZ computed gas phase XYZ coordinates for all GS structures (Table S5), CAM-B3LYP/cc-pVTZ computed gas phase XYZ coordinates for all ES structures (Table S6), CAM-B3LYP/cc-pVTZ optimized structures of compounds **1** and **2** in the gas phase and in solution (methanol) for both GS and ES (Figure S1), PBE0/cc-pVTZ optimized gas phase structures in the GS (Figure S2), CAM-B3LYP/cc-pVTZ optimized gas phase structures in the

DOI: 10.1021/ct500775r
J. Chem. Theory Comput. 2015, 11, 2619−2632

GS (Figure S3), CAM-B3LYP/cc-pVTZ optimized gas phase structures in the ES (Figure S4), EDD plots for all of the studied systems (Figure S5), CASSCF optimized orbitals included in the active spaces of compounds **1**−**16** (Figures S6−S22, respectively), frontier molecular orbitals of the GS for all of the studied systems (Figures S23−S26, respectively). The Supporting Information is available free of charge on the ACS Publications website at DOI: 10.1021/ct500775r.

AUTHOR INFORMATION

Corresponding Author

*E-mail: alex.brown@ualberta.ca.

Funding

We thank the Natural Sciences and Engineering Research Council (NSERC) of Canada for financial support and the Canadian Foundation for Innovation (New Opportunities Fund) for support for computational infrastructure.

Notes

The authors declare no competing financial interest.

ACKNOWLEDGMENTS

This research has been (partially) enabled by the use of computing resources provided by WestGrid and Compute/Calcul Canada. We also thank E. Peña-Cabrera (Universidad de Guanajuato) for providing the data for the experimental absorption spectra presented in Figure 3. M.R.M. gratefully acknowledges Farnaz A. Shakib for her help during preparation of this work. We thank the reviewers for insightful comments and suggestions.

REFERENCES

(1) Loudet, A.; Burgess, K. *Chem. Rev.* **2007**, *107*, 4891−4932.
(2) Ulrich, G.; Ziessel, R.; Harriman, A. *Angew. Chem., Int. Ed.* **2008**, *47*, 1184−1201.
(3) Kamkaew, A.; Lim, S. H.; Lee, H. B.; Kiew, L. V.; Chung, L. Y.; Burgess, K. *Chem. Soc. Rev.* **2013**, *42*, 77−88.
(4) Awuah, S. G.; You, Y. *RSC Adv.* **2012**, *2*, 11169−11183.
(5) Nepomnyashchii, A. B.; Bard, A. J. *Acc. Chem. Res.* **2012**, *45*, 1844−1853.
(6) López Arbeloa, F.; Bañuelos, J.; Martínez, V.; Arbeloa, T.; López Arbeloa, I. *Int. Rev. Phys. Chem.* **2005**, *24*, 339−374.
(7) Duran-Sampedro, G.; Agarrabeitia, A. R.; Garcia-Moreno, I.; Costela, A.; Bañuelos, J.; Arbeloa, T.; López Arbeloa, I.; Chiara, J. L.; Ortiz, M. J. *Eur. J. Org. Chem.* **2012**, *2012*, 6335−6350.
(8) Boens, N.; Leen, V.; Dehaen, W. *Chem. Soc. Rev.* **2012**, *41*, 1130−1172.
(9) Gonçalves, M. S. T. *Chem. Rev.* **2009**, *109*, 190−212.
(10) Yuan, L.; Lin, W.; Zheng, K.; He, L.; Huang, W. *Chem. Soc. Rev.* **2013**, *42*, 622−661.
(11) Vendrell, M.; Zhai, D.; Er, J. C.; Chang, Y.-T. *Chem. Rev.* **2012**, *112*, 4391−4420.
(12) Batat, P.; Cantuel, M.; Jonusauskas, G.; Scarpantonio, L.; Palma, A.; O'Shea, D. F.; McClenaghan, N. D. *J. Phys. Chem. A* **2011**, *115*, 14034−14039.
(13) Treibs, V. A.; Kreuzer, F. H. *Liebigs Ann. Chem.* **1968**, *718*, 208−223.
(14) Schmitt, A.; Hinkeldey, B.; Wild, M.; Jung, G. *J. Fluoresc.* **2009**, *19*, 755−758.
(15) Arroyo, I. J.; Hu, R.; Merino, G.; Tang, B. Z.; Peña-Cabrera, E. *J. Org. Chem.* **2009**, *74*, 5719−5722.
(16) Ni, Y.; Zeng, W.; Huang, K.-W.; Wu, J. *Chem. Commun. (Cambridge, U. K.)* **2013**, *49*, 1217−1219.
(17) Gresser, R.; Hartmann, H.; Wrackmeyer, M.; Leo, K.; Riede, M. *Tetrahedron* **2011**, *67*, 7148−7155.
(18) Hayashi, Y.; Obata, N.; Tamaru, M.; Yamaguchi, S.; Matsuo, Y.; Saeki, A.; Seki, S.; Kureishi, Y.; Saito, S.; Yamaguchi, S.; Shinokubo, H. *Org. Lett.* **2012**, *14*, 866−869.
(19) Jiang, X.-D.; Fu, Y.; Zhang, T.; Zhao, W. *Tetrahedron Lett.* **2012**, *53*, 5703−5706.
(20) Yu, C.; Xu, Y.; Jiao, L.; Zhou, J.; Wang, Z.; Hao, E. *Chem.—Eur. J.* **2012**, *18*, 6437−6442.
(21) Berhe, S. A.; Rodriguez, M. T.; Park, E.; Nesterov, V. N.; Pan, H.; Youngblood, W. J. *Inorg. Chem.* **2014**, *53*, 2346−2348.
(22) Sarkar, S. K.; Mukherjee, S.; Thilagar, P. *Inorg. Chem.* **2014**, *53*, 2343−2345.
(23) Le Guennic, B.; Maury, O.; Jacquemin, D. *Phys. Chem. Chem. Phys.* **2012**, *14*, 157−164.
(24) Céron-Carrasco, J. P.; Siard, A.; Jacquemin, D. *Dyes Pigm.* **2013**, *99*, 972−978.
(25) Chibani, S.; Le Guennic, B.; Charaf-Eddin, A.; Maury, O.; Andraud, C.; Jacquemin, D. *J. Chem. Theory Comput.* **2012**, *8*, 3303−3313.
(26) Chibani, S.; Charaf-Eddin, A.; Mennucci, B.; Le Guennic, B.; Jacquemin, D. *J. Chem. Theory Comput.* **2014**, *10*, 805−815.
(27) Chibani, S.; Charaf-Eddin, A.; Le Guennic, B.; Jacquemin, D. *J. Chem. Theory Comput.* **2013**, *9*, 3127−3135.
(28) Le Guennic, B.; Chibani, S.; Charaf-Eddin, A.; Massue, J.; Ziessel, R.; Ulrich, G.; Jacquemin, D. *Phys. Chem. Chem. Phys.* **2013**, *15*, 7534−7540.
(29) Charaf-Eddin, A.; Le Guennic, B.; Jacquemin, D. *Theor. Chem. Acc.* **2014**, *133*, 1−9.
(30) Chibani, S.; Le Guennic, B.; Charaf-Eddin, A.; Laurent, A. D.; Jacquemin, D. *Chem. Sci.* **2013**, *4*, 1950−1963.
(31) Boulanger, P.; Chibani, S.; Le Guennic, B.; Duchemin, I.; Blase, X.; Jacquemin, D. *J. Chem. Theory Comput.* **2014**, *10*, 4548−4556.
(32) Chibani, S.; Laurent, A. D.; Le Guennic, B.; Jacquemin, D. *J. Chem. Theory Comput.* **2014**, *10*, 4574−4582.
(33) Charaf-Eddin, A.; Le Guennic, B.; Jacquemin, D. *RSC Adv.* **2014**, *4*, 49449−49456.
(34) Rhee, Y. M.; Head-Gordon, M. *J. Phys. Chem. A* **2007**, *111*, 5314−5326.
(35) Goerigk, L.; Grimme, S. *J. Chem. Phys.* **2010**, *132*, No. 184103.
(36) Petrushenko, I.; Petrushenko, K. *Spectrochim. Acta, Part A* **2015**, *138*, 623−627.
(37) Le Guennic, B.; Jacquemin, D. *Acc. Chem. Res.* **2015**, *48*, 530−537.
(38) Perdew, J. P.; Burke, K.; Ernzerhoff, M. *Phys. Rev. Lett.* **1996**, *77*, 3865−3868.
(39) Perdew, J. P.; Burke, K.; Ernzerhoff, M. *Phys. Rev. Lett.* **1996**, *78*, 1396−1396.
(40) Adamo, C.; Barone, V. *J. Chem. Phys.* **1999**, *110*, 6158−6169.
(41) Yanai, T.; Tew, D. P.; Handy, N. C. *Chem. Phys. Lett.* **2004**, *393*, 51−57.
(42) Dunning, T. H., Jr. *J. Chem. Phys.* **1990**, *90*, 1007−1023.
(43) Woon, D. E.; Dunning, T. H., Jr. *Chem. Phys.* **1993**, *98*, 1358−1371.
(44) Jacquemin, D.; Planchat, A.; Adamo, C.; Mennucci, B. *J. Chem. Theory Comput.* **2012**, *8*, 2359−2372.
(45) Jacquemin, D.; Wathelet, V.; Perpète, E. A.; Adamo, C. *J. Chem. Theory Comput.* **2009**, *5*, 2420−2435.
(46) Cances, E.; Mennucci, B.; Tomasi, J. *J. Chem. Phys.* **1997**, *107*, 3032−3041.
(47) Cossi, M.; Scalmani, G.; Rega, N.; Barone, V. *J. Chem. Phys.* **2002**, *117*, 43−54.
(48) Becke, A. D. *Phys. Rev. A* **1988**, *38*, 3098−3100.
(49) Lee, C.; Yang, W.; Parr, R. G. *Phys. Rev. B* **1988**, *37*, 785−789.
(50) Miehlich, B.; Savin, A.; Stoll, H.; Preuss, H. *Chem. Phys. Lett.* **1989**, *157*, 200−206.
(51) Adamo, C.; Barone, V. *Chem. Phys. Lett.* **1997**, *274*, 242−250.
(52) Becke, A. *J. Chem. Phys.* **1996**, *104*, 1040−1046.
(53) Iikura, H.; Tsuneda, T.; Yanai, T.; Hirao, K. *J. Chem. Phys.* **2001**, *115*, 3540−3544.

DOI: 10.1021/ct500775r
J. Chem. Theory Comput. 2015, 11, 2619−2632

(54) Chai, J.-D.; Head-Gordon, M. *Phys. Chem. Chem. Phys.* **2008**, *10*, 6615−6620.
(55) Vydrov, O. A.; Scuseria, G. E. *J. Chem. Phys.* **2006**, *125*, No. 234109.
(56) Vydrov, O. A.; Heyd, J.; Krukau, A. V.; Scuseria, G. E. *J. Chem. Phys.* **2006**, *125*, No. 074106.
(57) Vydrov, O. A.; Scuseria, G. E.; Perdew, J. P. *J. Chem. Phys.* **2007**, *126*, No. 154109.
(58) Foresman, J. B.; Head-Gordon, M.; Pople, J. A.; Frisch, M. J. *J. Phys. Chem.* **1992**, *96*, 135−149.
(59) Head-Gordon, M.; Rico, R. J.; Oumi, M.; Lee, T. J. *Chem. Phys. Lett.* **1994**, *219*, 21−29.
(60) Koch, H.; Jorgensen, P. *J. Chem. Phys.* **1990**, *93*, 3333−3344.
(61) Stanton, J. F.; Bartlett, R. J. *J. Chem. Phys.* **1993**, *98*, 7029−7039.
(62) Koch, H.; Kobayashi, R.; Sanchez de Merás, A.; Jorgensen, P. *J. Chem. Phys.* **1994**, *100*, 4393−4400.
(63) Kállay, M.; Gauss, J. *J. Chem. Phys.* **2004**, *121*, 9257−9269.
(64) Kats, D.; Schütz, M. *J. Chem. Phys.* **2009**, *131*, No. 124117.
(65) Freundorfer, K.; Kats, D.; Korona, T.; Schütz, M. *J. Chem. Phys.* **2010**, *133*, No. 244110.
(66) Nakatsuji, H. *Chem. Phys. Lett.* **1979**, *67*, 334−342.
(67) Widmark, P.-O.; Malmqvist, P.-Å; Roos, B. O. *Theor. Chem. Acc.* **1990**, *77*, 291−306.
(68) Celani, P.; Werner, H.-J. *J. Chem. Phys.* **2000**, *112*, 5546−5557.
(69) Forsberg, N.; Malmqvist, P.-Å. *Chem. Phys. Lett.* **1997**, *274*, 196−204.
(70) Kendall, R. A.; Dunning, T. H., Jr.; Harrison, R. J. *J. Chem. Phys.* **1992**, *96*, 6796−6806.
(71) Le Bahers, T.; Adamo, C.; Ciofini, I. *J. Chem. Theory Comput.* **2011**, *7*, 2498−2506.
(72) Jacquemin, D.; Bahers, T. L.; Adamo, C.; Ciofini, I. *Phys. Chem. Chem. Phys.* **2012**, *14*, 5383−5388.
(73) Cižek, J. In *Advances in Chemical Physics*; Hariharan, P. C., Ed.; Wiley Interscience: New York, 1969; Vol. *14*; p 35.
(74) Purvis, G. D.; Bartlett, R. J. *J. Chem. Phys.* **1982**, *76*, 1910−1918.
(75) Scuseria, G. E.; Janssen, C. L.; Schaefer, H. F. *J. Chem. Phys.* **1988**, *89*, 7382−7387.
(76) Scuseria, G. E.; Schaefer, H. F. *J. Chem. Phys.* **1989**, *90*, 3700−3703.
(77) Pople, J. A.; Head-Gordon, M.; Raghavachari, K. *J. Chem. Phys.* **1987**, *87*, 5968−5975.
(78) Lee, T. J.; Taylor, P. R. *Int. J. Quantum Chem. Symp.* **1989**, *23*, 199−207.
(79) Karton, A.; Rabinovich, E.; Martin, J. M. L.; Ruscic, B. *J. Chem. Phys.* **2006**, *125*, No. 144108.
(80) Tishchenko, O.; Zheng, J.; Truhlar, D. G. *J. Chem. Theory Comput.* **2008**, *4*, 1208−1219.
(81) Frisch, M. J.; Trucks, G. W.; Schlegel, H. B.; Scuseria, G. E.; Robb, M. A.; Cheeseman, J. R.; Scalmani, G.; Barone, V.; Mennucci, B.; Petersson, G. A.; Nakatsuji, H.; Caricato, M.; Li, X.; Hratchian, H. P.; Izmaylov, A. F.; Bloino, J.; Zheng, G.; Sonnenberg, J. L.; Hada, M.; Ehara, M.; Toyota, K.; Fukuda, R.; Hasegawa, J.; Ishida, M.; Nakajima, T.; Honda, Y.; Kitao, O.; Nakai, H.; Vreven, T.; Montgomery, J. A., Jr.; Peralta, J. E.; Ogliaro, F.; Bearpark, M.; Heyd, J. J.; Brothers, E.; Kudin, K. N.; Staroverov, V. N.; Kobayashi, R.; Normand, J.; Raghavachari, K.; Rendell, A.; Burant, J. C.; Iyengar, S. S.; Tomasi, J.; Cossi, M.; Rega, N.; Millam, M. J.; Klene, M.; Knox, J. E.; Cross, J. B.; Bakken, V.; Adamo, C.; Jaramillo, J.; Gomperts, R.; Stratmann, R. E.; Yazyev, O.; Austin, A. J.; Cammi, R.; Pomelli, C.; Ochterski, J. W.; Martin, R. L.; Morokuma, K.; Zakrzewski, V. G.; Voth, G. A.; Salvador, P.; Dannenberg, J. J.; Dapprich, S.; Daniels, A. D.; Farkas, Ö; Foresman, J. B.; Ortiz, J. V.; Cioslowski, J.; Fox, D. J. *Gaussian 09*, Revision B.1; Gaussian: Wallingford, CT, USA, 2009.
(82) Werner, H.-J.; Knowles, P. J.; Knizia, G.; Manby, F. R.; Schütz, M.; Celani, P.; Korona, T.; Lindh, R.; Mitrushenkov, A.; Rauhut, G.; Shamasundar, K. R.; Adler, T. B.; Amos, R. D.; Bernhardsson, A.; Berning, A.; Cooper, D. L.; Deegan, M. J. O.; Dobbyn, A. J.; Eckert, F.; Goll, E.; Hampel, C.; Hesselmann, A.; Hetzer, G.; Hrenar, T.; Jansen, G.; Köppl, C.; Liu, Y.; Lloyd, A. W.; Mata, R. A.; May, A. J.; McNicholas, S. J.; Meyer, W.; Mura, M. E.; Nicklass, A.; O'Neill, D. P.; Palmieri, P.; Peng, D.; Pflüger, K.; Pitzer, R.; Reiher, M.; Shiozaki, T.; Stoll, H.; Stone, A. J.; Tarroni, R.; Thorsteinsson, T.; Wang, M. *MOLPRO, version 2012.1, a package of ab initio programs*, 2012; see http://www.molpro.net (accessed Dec. 1, 2014) .
(83) *DALTON2013, a molecular electronic structure program*, 2013; see http://www.daltonprogram.org (accessed Dec. 1, 2014).
(84) Zhao, W.; Carreira, E. M. *Chem.—Eur. J.* **2006**, *12*, 7254−7263.
(85) Uppsten, M.; Durbeej, B. *J. Comput. Chem.* **2012**, *33*, 1892−1901.
(86) Mao, M.; Xiao, S.; Yi, T.; Zou, K. *J. Fluorine Chem.* **2011**, *132*, 612−616.
(87) Ross, T. W.; Sathyamoorthi, G.; Boyer, J. H. *Heteroat. Chem.* **1993**, *4*, 609−612.
(88) Bañuelos, J.; Arbeloa, F. L.; Martinez, V.; Liras, M.; Costela, A.; Moreno, I. G.; Arbeloa, I. L. *Phys. Chem. Chem. Phys.* **2011**, *13*, 3437−3445.
(89) Wu, L.; Burgess, K. *J. Am. Chem. Soc.* **2008**, *130*, 4089−4096.
(90) Baranov, M. S.; Lukyanov, K. A.; Borissova, A. O.; Shamir, J.; Kosenkov, D.; Slipchenko, L. V.; Tolbert, L. M.; Yampolsky, I. V.; Solntsev, K. M. *J. Am. Chem. Soc.* **2012**, *134*, 6025−6032.
(91) Osorio-Martínez, C. A.; Urías-Benavides, A.; Gómez-Durán, C. F. A.; Bañuelos, J.; Esnal, I.; López Arbeloa, I.; Peña-Cabrera, E. *J. Org. Chem.* **2012**, *77*, 5434−5438.
(92) Sathyamoorthi, G.; Boyer, J. H.; Allik, T. H.; Chandra, S. *Heteroat. Chem.* **1994**, *5*, 403−407.
(93) Kubota, Y.; Tsuzuki, T.; Funabiki, K.; Ebihara, M.; Matsui, M. *Org. Lett.* **2010**, *12*, 4010−4013.
(94) Ziessel, R.; Goze, C.; Ulrich, G. *Synthesis* **2007**, 936−949.
(95) Goud, T. V.; Tutar, A.; Biellmann, J.-F. *Tetrahedron* **2006**, *62*, 5084−5091.
(96) Boyer, J. H.; Haag, A. M.; Sathyamoorthi, G.; Soong, M.-L.; Thangaraj, K.; Pavlopoulos, T. G. *Heteroat. Chem.* **1993**, *4*, 39−49.
(97) Walczak, E.; Szefczyk, B.; Andruniów, T. *J. Chem. Theory Comput.* **2013**, *9*, 4915−4927.
(98) Send, R.; Kühn, M.; Furche, F. *J. Chem. Theory Comput.* **2011**, *7*, 2376−2386.
(99) Goerigk, L.; Moellmann, J.; Grimme, S. *Phys. Chem. Chem. Phys.* **2009**, *11*, 4611−4620.
(100) Barone, V.; Bloino, J.; Biczysko, M.; Santoro, F. *J. Chem. Theory Comput.* **2009**, *5*, 540−554.
(101) Gorelsky, S. *AOMix: Program for Molecular Orbital Analysis*, version 6.X; University of Ottawa, Ottawa, Canada, 2013, http://www.sg-chem.net/ (accessed Dec. 1, 2014).
(102) Gorelsky, S.; Lever, A. *J. Organomet. Chem.* **2001**, *635*, 187−196.
(103) Tozer, D. J. *J. Chem. Phys.* **2003**, *119*, 12697−12699.
(104) Dreuw, A.; Head-Gordon, M. *J. Am. Chem. Soc.* **2004**, *126*, 4007−4016.
(105) Grimme, S.; Neese, F. *J. Chem. Phys.* **2007**, *127*, No. 154116.
(106) Briggs, E. A.; Besley, N. A.; Robinson, D. *J. Phys. Chem. A* **2013**, *117*, 2644−2650.
(107) Buyuktemiz, M.; Duman, S.; Dede, Y. *J. Phys. Chem. A* **2013**, *117*, 1665−1669.
(108) Cakmak, Y.; Kolemen, S.; Duman, S.; Dede, Y.; Dolen, Y.; Kilic, B.; Kostereli, Z.; Yildirim, L. T.; Dogan, A. L.; Guc, D.; Akkaya, E. U. *Angew. Chem., Int. Ed.* **2011**, *50*, 11937−11941.
(109) Valiev, R. R.; Sinelnikov, A. N.; Aksenova, Y. V.; Kuznetsova, R. T.; Berezin, M. B.; Semeikin, A. S.; Cherepanov, V. N. *Spectrochim. Acta, Part A* **2014**, *117*, 323−329.
(110) Jiang, X.-D.; Zhang, H.; Zhang, Y.; Zhao, W. *Tetrahedron* **2012**, *68*, 9795−9801.
(111) Tanaka, K.; Yamane, H.; Yoshii, R.; Chujo, Y. *Bioorg. Med. Chem.* **2013**, *21*, 2715−2719.
(112) Killoran, J.; Allen, L.; Gallagher, J. F.; Gallagher, W. M.; ÓShea, D. F. *Chem. Commun. (Cambridge, U.K.)* **2002**, 1862−1863.
(113) Bellier, Q.; Pégaz, S.; Aronica, C.; Guennic, B. L.; Andraud, C.; Maury, O. *Org. Lett.* **2011**, *13*, 22−25.

DOI: 10.1021/ct500775r
J. Chem. Theory Comput. 2015, 11, 2619−2632

(114) Bouit, P.-A.; Kamada, K.; Feneyrou, P.; Berginc, G.; Toupet, L.; Maury, O.; Andraud, C. *Adv. Mater.* **2009**, *21*, 1151−1154.
(115) Gorman, A.; Killoran, J.; O'Shea, C.; Kenna, T.; Gallagher, W. M.; O'Shea, D. F. *J. Am. Chem. Soc.* **2004**, *126*, 10619−10631.
(116) Jiao, L.; Wu, Y.; Wang, S.; Hu, X.; Zhang, P.; Yu, C.; Cong, K.; Meng, Q.; Hao, E.; Vicente, M. G. H. *J. Org. Chem.* **2014**, *79*, 1830−1835.
(117) Moore, B., II; Autschbach, J. *J. Chem. Theory Comput.* **2013**, *9*, 4991−5003.

DOI: 10.1021/ct500775r
J. Chem. Theory Comput. 2015, 11, 2619−2632